Chin.J.Geochem.(2014)33:065–076
DOI: 10.1007/s11631-014-0660-8

Fluid inclusion, siliceous rock geochemistry of Shewushan lateritic gold deposit, Hubei Province, eastern China: Implication for the genesis of primary orebody

WANG Minfang[1,2*], ZHENG Youye[1,2], XU Rongke[3], LIU Yunguang[4], XIAO Fan[5], CHENG Shanwen[6], and SUN Xiangmin[7]

[1] *Faculty of Earth Resources, China University of Geosciences, Wuhan 430074, China*

[2] *State Key Laboratory of Geological Processes and Mineral Resources, China University of Geosciences, Wuhan 430074, China*

[3] *Institute of Geological Survey, China University of Geosciences, Wuhan 430074, China*

[4] *Sichuan Institute of Nuclear Geology, Chengdu 610051, China*

[5] *Nanjing Center, China Geological Survey, Nanjing 210016, China*

[6] *Shewushan Gold Mine Co. Ltd, Xianning 437000, China*

[7] *No. 4 Geological Party, Hubei Bureau of Geology and Mineral Resources, Xianning 437000, China*

[*] *Corresponding author, E-mail: wang_minfang@163.com*

Received May 20, 2013; accepted July 12, 2013

Abstract The Shewushan gold deposit is located 16 km southwest of Jiayu County, Hubei Province, eastern China, which is the largest lateritic gold deposit in Asia, consisting of a series of mineralized faults containing gold grades of 1.0–19.5 g/t set within a larger, lower-grade (0.2–1.0 g/t) zone. According to the fluid inclusions study, the homogenization temperature ranges from 70–350℃, and concentrates between 140–220℃. The laser Rama results show that the CO_2 and CH_4 exist in mineralized fluid. In addition, the major and trace element and REE geochemical data show that the genesis of the siliceous rocks is hydrothermal genesis, formed by mineralized fluid bearing SiO_2 transmitted along faults to the surface, and replace the carbonate rocks to begin deposition. Primary gold mineralization is attributed to hydrothermal activity that followed the main period of tectonic deformation of the Indosinian orogeny, which caused the regional detachment regime in southeast Hubei. The reversed fold and the fault system formed the fluid migration channel in the Shewushan area. EPMA results show that Au exists in arsenopyrite (850×10^{-6}–1550×10^{-6} Au) and pyrite (470×10^{-6}–1340×10^{-6} Au). Therefore, based on the above results and combined with the field observation, we suggest that the genesis of primary orebody in Shewushan deposit is carlin type, while not weathered residual type.

Key words siliceous rock; carlin type; primary orebody; Shewushan gold deposit; eastern China

1 Introduction

Since the first discovery of the Boddington lateritic gold deposit in Western Australian and the discovery of the second large-scale Bahia lateritic gold deposit in Brazil in 1980's (Davy, 1979; Davy and El-Ansary, 1986; Zang Weisheng and Fyfe, 1993), intensive prospecting for lateritic gold deposits have been undertaken in many countries, such as Brazil (Zang Weisheng and Fyfe, 1993; Porto and Hale, 1995; Varajão et al., 2000; Larizzatti et al., 2008), India (Santosh and Omana, 1991), South America (Marcondes, 1993), Western Africa (Freyssinet et al., 1989) and Australia (Glasson et al., 1988). Lateritic type gold deposits, have received worldly attentions from then on due to its apparent advantages of large scales (middle-large to ultra-large type ore mines), readily exploitation (with loose mine layers and open pit), easy milling and metallurgy, especially higher extraction ratios (larger than 75%) and great investment incomes (Yang Yuangen et al., 2009). Investigations revealed that a number of lateritic gold deposits are situated in the tropics where extensive lateritic terrains have existed since the Tertiary in inner tropical zones covered by dense rain forests. Laterites were formed in places such as the Amazon region and West Africa (Lima da Costa, 1993; Zang Weisheng and Fyfe, 1993).

In China, this kind of gold deposits has been paid more attention (Cao Xinzhi, 1998; Tu Guangchi, 1999; Chen Dajing and Yang Mingshou, 1999; Wang Yan and Tan Kaixuan, 2002). Shewushan gold deposit is the first discovered lateritic gold deposit in eastern China and the largest in Asia. A series of lateritic gold deposits had been found in succession from the end of 1980's to the beginning of 1990's, and have become an important type of gold resource in China (Cao Xinzhi, 1998; Chen Dajing et al., 2001; Wang Yan and Tan Kaixuan, 2002). However, both climate and tectonic settings in Shewushan are different from the area where typical lateritic gold deposits located. For example, the climate is warm and humid in the Shewushan area. The annual rainfall is ~1100 mm, mainly between April and October, and the average temperature is 18℃, with a mean of 4.1℃ during the coldest month (January) and 29.2℃ during the warmest month (July) of a year. The landscape consists of hills covered with evergreen trees and bushes and comprises relatively flat aggraded and coalesced alluvial fans, with the base level of erosion 20 m above mean sea level (Hong Hanlie and Tie Liyun, 2005). The intensive tectonic movement during the Cenozoic limited the development of an erosional plain, and most of the bedrock is primary carbonates. As a result, the particle size of the gold in the weathering profile is extremely small; most grains are <0.02 mm in size and occur at the rims of clay mineral grains (Hong Hanlie, 1996, 1999).

Previous studies of the Shewushan gold deposit mainly focused on the geological conditions, geochemical characteristics, and genetic model of this type of weathering-related gold deposit (Li Songsheng, 1993; Li Jiangyuan et al., 1994; Yu Renyu, 1994; Liu Tengfei, 1996; Hong Hanlie et al., 2000). However, the genesis of the primary orebody is still uncertain. There exist two viewpoints on type of the genesis: weathered residual type (Yu Renyu, 1994; Li Songsheng, 1998) and carlin type (Li Jiaxiang and Liu Shimin, 1995; Liu Shimin and Li Jiaxiang, 1995). In this paper, we illustrate the genesis of the primary orebody by fluid inclusion and geochemistry study with electron microprobe analysis.

2 Geological background

The Shewushan gold deposit is located 16 km southwest of Jiayu County, Xianning City, Hubei Province, with reserve of approximately 10 Mt reserve and average grade of about 2.2 g/t (Fig. 1). Stratigraphic studies indicate that layers of the Cretaceous to the Tertiary are missing in the area, and erosion has taken place since the Cretaceous with upwards and downwards movement of the water table, perhaps due to seasonal changes, producing a redox environment and hence causing the dissolution and deposition of minerals in the weathering profile during the weathering process (Yu Renyu, 1994).

The geological setting of the Shewushan area has been interpreted through data gathered from drill holes (Ding Qixiu, 1992; Li Songsheng, 1993; Yu Renyu, 1994). The results show that an anticline is situated beneath the deposit with the axis of the Cambrian to the Ordovician limestone or dolostone and limbs of the Silurian to the Jurassic mudstone with limestone bands (Fig. 2). There exist a set of high-angle thrust folds trending east-west within the axis and the limbs. The major anticlinal axis generally trends east-west (around 100°) in the mine area.

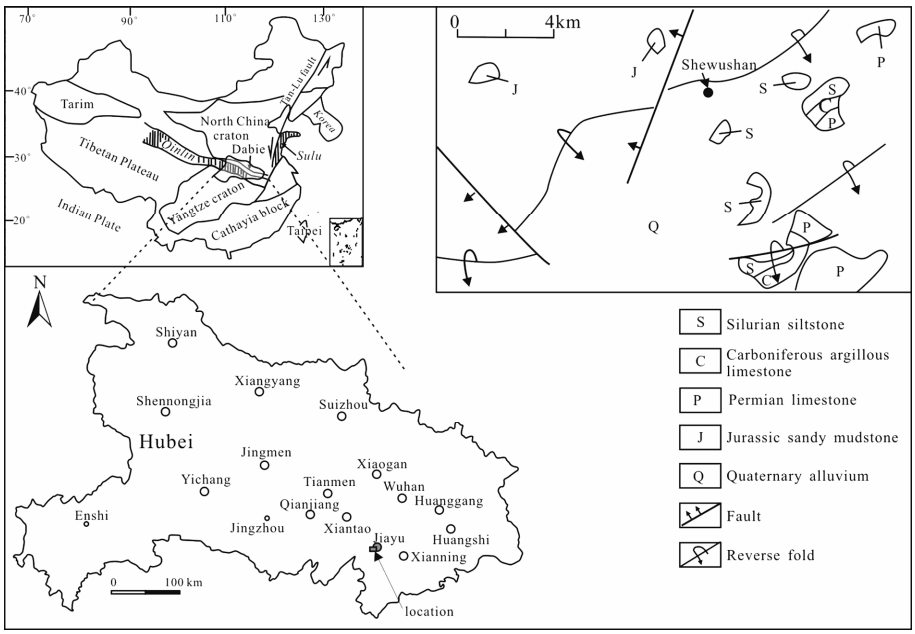

Fig. 1. Simplified mine geological map and location of Shewushan gold deposit (after Hong Hanlie, 2001).

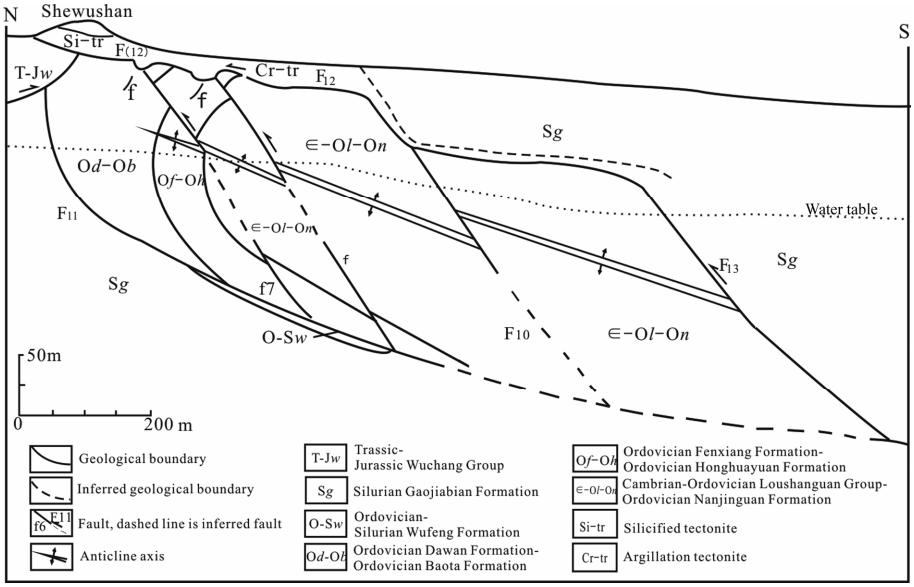

Fig. 2. The generalized model of the bimodal thrust faults in Shewushan gold deposit (modified from Wang Tong and Yang Mingai, 1992).

In addition, north-south-trending faults are the second important structure observed, with a set of faults oriented at 3°–8°, appearing postdate east-west faults and fractures thus probably postdate mineralization. The faults dip east at around 30°, showing local interference with the east-west structures especially, and offset silicified limestone (Fig. 3).

The structures in the deposit show features of multistage deformation. The east-west structures may represent the regional north-south-trending Indosinian orogeny in earlier stage. The north-south structures may be related to the later tectono-magmatic event with east-west maximum principal stress (Yu Renyu, 1996).

No igneous rocks are known to occur in the deposit, but there may be hidden igneous intrusion in the east of the deposit according to airborne magnetic survey data.

3 Mineralization and alteration

The elevation of the ore body occurrence is strongly controlled by structures, and the thickness and grade of the ore body increase in the fracture zone. The mineralization is confined to the structural area with the metasediments and crushed quartz veins and calcitization. East-west-trending fractures are most intense in the limestone, with a spacing of 5–60 cm (average 20 cm). The ore bodies are confined between the North Boundary Fault (F_{11}, with dip angle between 30–50°) and South Boundary Fault (F_{13}) (Fig. 4a, b), where developed crushed limestone and tectonic breccias (Fig. 4c, d). East-west-trending fractures occur as axial plane fanning fractures in fold crests. Away from the crests they are at high angle or even normal to bedding. Comb-textured or massive veins, which may be truncated by slip along the bedding or terminated against adjacent mudstone, which commonly fills such fractures.

Above the water table, silification, argillation, and ferritization occurred, whereas pyritization, realgarization, baritization, and bituminization occurred below the water table.

Silification is the wide spreading alteration in Shewushan gold deposit, which also called ‘silicon cap’ by on-site producers. It is limited to the faulted crushed zone and limestone units. The most intense areas of silification are the faulted crushed zones, where the massive siliceous rock occurs (Fig. 5a, b). It presents discontinuous shaped, trending mainly southwards and projecting at the surface for weathering. The areas of intense silification are generally related to a higher gold grade.

Argillation develops mainly in the weathering profile, where clay minerals occur in the matrix and fractures, with kaolinite and halloysite mainly in the upper portion and illite and minor kaolinite in the lower portion, which caused gold occurs within small Ag-bearing particles, nm-scale in size, adsorbed at the edges of illite and kaolinite (Wang Tong and Yang Mingai, 1992; Hong Hanlie, 1996; Hong Hanlie et al., 1999; Hong Hanlie and Tie Liyun, 2005).

Ferritization is the most intense surficial alteration in the mine. It is confined to weathering profile. Ferritization occurs as psendomorphs of the earlier sulfide (pyrite and marcasite), disseminated in the oxidized zone.

Pyritization develops widely in limestone, especially in western part of the mine, i.e., jarosite widely

occurs, implying pyritization development (Fig. 5c). In addition, realgarization develops together with orpiment (Fig. 5d). They could be recognized in the calcite vein or in limestone, which occurring as granulous or filmated in calcite vein (Fig. 5e), or being disseminated in limestone (Fig. 5f). Baritization occurs in vein or breccias, and coexists with calcite (Fig. 5g). Bituminization occurs in bedrock outcrop, which cement or cut calcite vein, later than calcite (Fig. 5h).

In brief, both hypogene and supergene mineralization are present in Shewushan gold deposit. The hypogene mineralization, i.e., primary mineralization, is closely associated with silification. Three silification stages are observed: 1) the first stage is barren, characteristically coplanar to the axial plane, and devoid of sulfides; 2) gold-bearing sulfide quartz veins and calcite veins postdating the first stage chalcedony quartz veins, which crosscut the former chalcedony quartz veins and probably represent the primary gold-bearing mineralization; 3) the third stage is characterized by the disrupting of sulfide quartz veins and calcite veins by barite quartz veins.

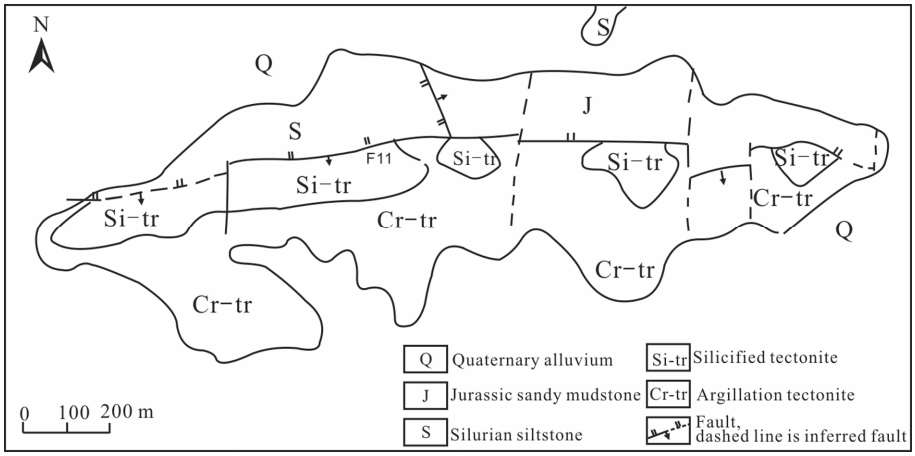

Fig. 3. Geological sketch map showing mine structure and lithology in Shewushan gold deposit.

Fig. 4. Characteristics observed in the field. a. North Boundary Fault (F_{11}), about 120° trending; b. South Boundary Fault (F_{13}); c. crushed limestone near F_{13}; d. tectonic breccias occurs near F_{11}.

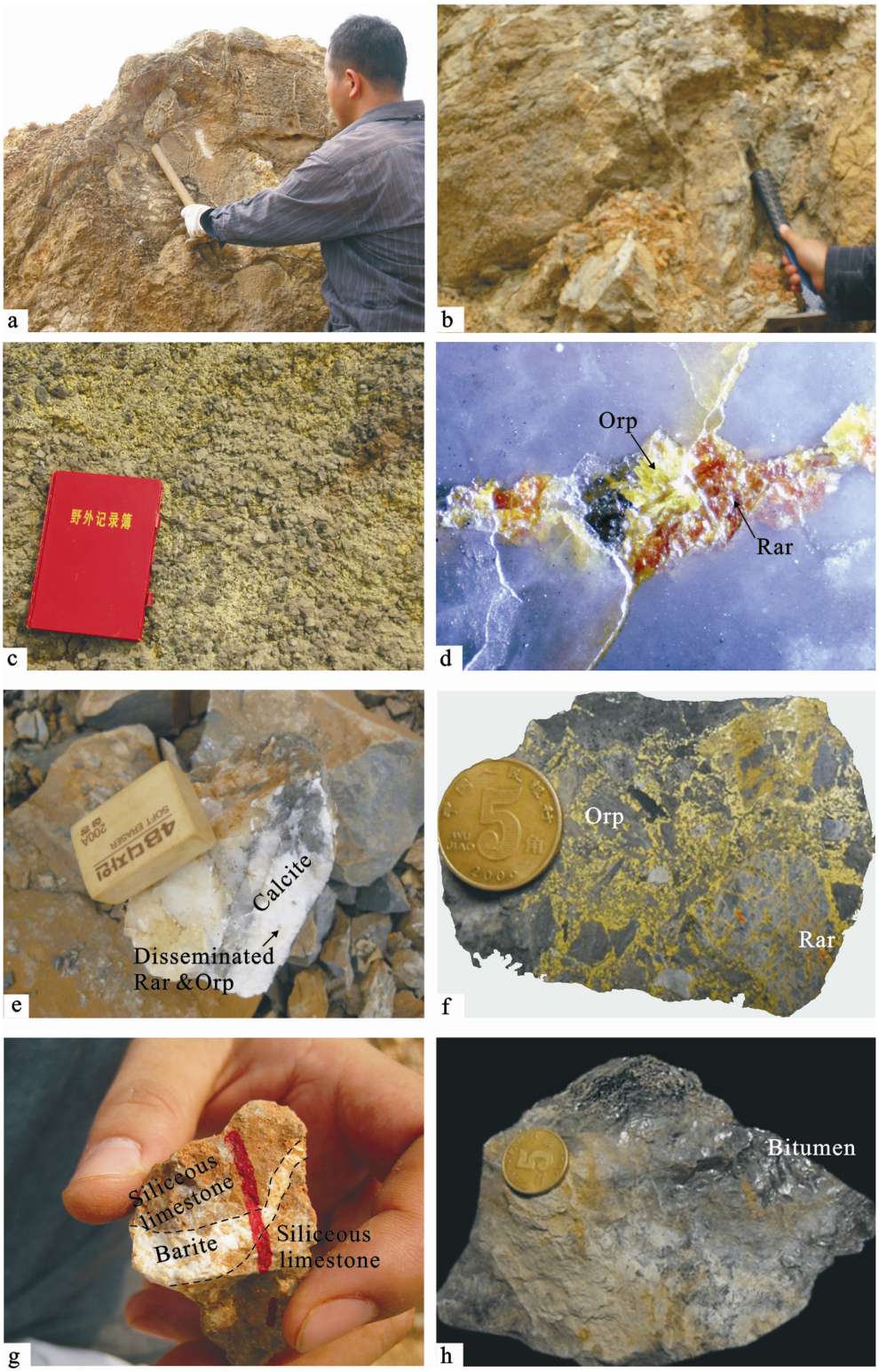

Fig. 5. Various alterations in Shewushan gold deposit. a. Chalcedony cement brecciaous limestone in F_{13} fault crushed zone; b. silicified limestone (primary mineralized bodies) outcrop in F_{13} fault crushed zone; c. jarosite widely occurs in western part of ore mine; d. realgarization coexist with orpiment in polished section with oblique light, five times magnification; e. realgarization, orpiment disseminated occurs in calcite vein in F_{11} fault zone; f. realgarization and orpiment in brecciaous limestone; g. barite cut across the siliceous limestone; h. bitumen envelope the calcite in F_{11} fault zone; Rar. reaglar; Orp. orpiment.

4. Fluid inclusion studies

4.1 Petrography and homogenization temperature

Nineteen samples were observed for homogenization temperature at Fluid Inclusion Laboratory in China University of Geosciences (Wuhan). The location of the samples could be seen in Fig 6. Limestone, dolomite, cryptite and silicite samples were collected from outcrop. These samples were cut and double polished into around 0.3 mm thick sections to observe.

All of the three types' inclusions have been observed in samples, i.e. primary (Fig. 7a, b), pseudosecondary (Fig. 7c) and secondary (Fig. 7d) fluid inclusions. Primary inclusions are typically larger (maximum 20 μm) and isolated. Pseudosecondary and secondary fluid inclusions define linear trails and are much smaller (typically <5 μm) (Fig. 7c, d). Analysis was in most cases confined to inclusions thought to be of primary origin and hence allows us to document temperature in mineralized fluid.

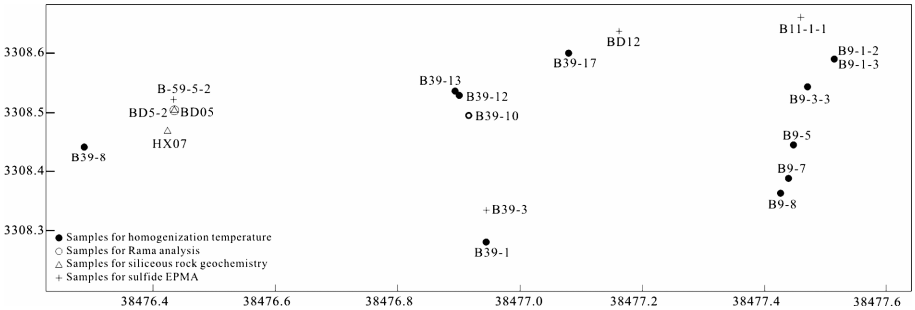

Fig. 6. Samples distribution in Shewushan deposit.

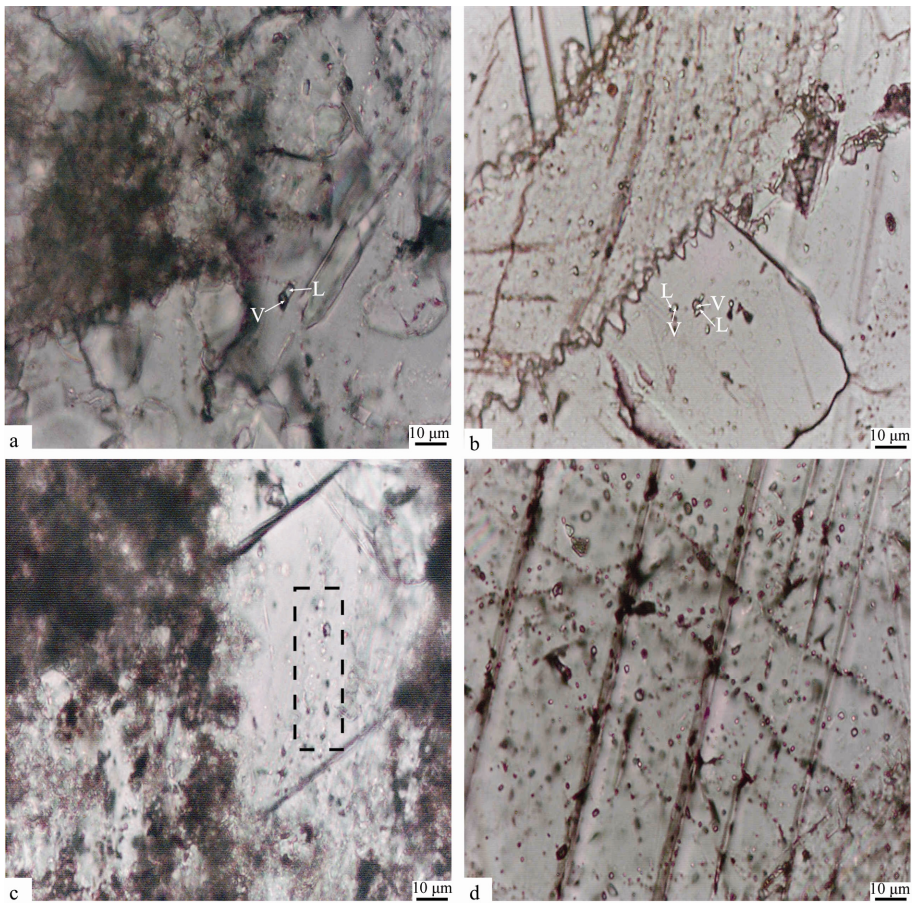

Fig. 7. Fluid inclusion petrography in Shewushan gold deposit. a. Primary fluid inclusion with isolated occurrence; b. primary fluid inclusion in small clusters; c. pseudosecondary fluid inclusion distributed in calcite fissure; d. secondary fluid inclusion in calcite fissures.

There are two kinds of inclusions exist, i.e. aqueous (most abundant) fluid inclusions and CO_2-rich fluid inclusions. For the first type, the vapor phase occupies 5% to 10%, and to a lesser extent 15% to 40% of the total volume of individual inclusions. They are in mostly irregular and elliptic shape. Most of them are less than 8 μm in diameter; some are large, reaching 20 μm for the longest dimension. They occurred either in the small cluster without obvious planar orientation or in wide hands. The homogenization temperatures range from 70 to 350℃, concentrating between 140 and 220℃, which is middle-low temperature (Fig. 8).

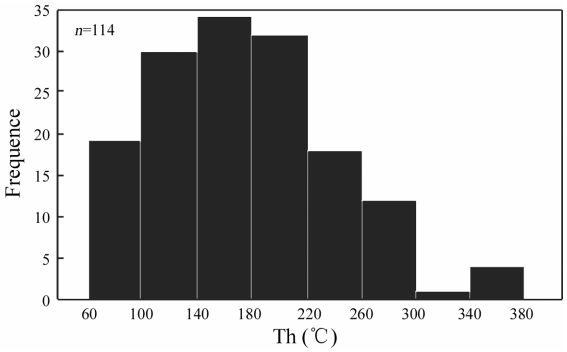

Fig. 8. Histogram showing homogenization temperatures of aqueous fluid inclusions in Shewushan gold deposit.

At the room temperature, these CO_2-rich fluid inclusions contain liquid and vapor carbonic phase and an aqueous liquid phase. These inclusions have a dark appearance, and therefore, the boundary between the liquid and vapor carbonic phase is not always evident. According to the previous study by Liu Shimin and Li Jiaxiang (1995), the salinity ranges from 2.2 to 9.34 wt.%, and the density ranges from 0.817 to 0.990 g/cm^3, with pressure from 42 to 46 MPa, showing low salinity and high density fluid characteristics, which implies the forming depth is about 1.5–2 km (Liu Shimin and Li Jiaxiang, 1995).

4.2 Laser Rama spectroscopy

To define the gas content in hydrothermal fluids, nine samples were analyzed using a laser Raman microprobe at the State Key Laboratory of Geological Processes and Mineral Resources, China University of Geosciences. The fluid inclusions were synthesized according to the experimental method described by Bodnar and Sterner (1987). Laser Raman spectroscopic measurements were done with a Renishaw RM 1000 instrument, made by Renishaw Company in United Kingdom. Raman measurement was conducted by using a microscopic confocal Raman spectrometer at room temperature. The 514.5-nm line of an Ar-ion laser with a power of about 3 mW was used to excite the Raman spectra. The diameter of the laser spot focused on the sample was ca. 25 μm. The resolution of the Raman spectra was 1 cm^{-1}.

Suitable samples were picked up for Rama determination, i.e., BD5-2 (barite) and B39-10 (silicified recrystallized limestone). There are three spots in two samples have determined the CO_2 and CH_4 at the room temperature in the Raman spectra (Fig. 9), suggesting the reducing fluid.

5 Geochemistry of siliceous rock

5.1 Sample and method

Silification is the wide developing and important alteration associated with gold mineralization. We collected laminate-lenticular siliceous rocks in the field. Samples were washed with distilled water, and were ground and passed through a 75 μm mesh sieve. After desiccation, major elements were analyzed in the Australian Laboratory Services (ALS) CHEMX, Guangzhou, China, and trace and rare earth elements (REE) were analyzed in the State Key Laboratory of Geological Processes and Mineral Resources, China University of Geosciences. Major oxides were determined by wavelength-dispersive X-ray fluorescence spectrometry (XRF) of fused with lithium metaborite. The trace elements, including REE, were determined by ICP-MS using a GeoLas 2005 system, and an Agilent 7500a ICP-MS instrument was used to acquire ion-signal intensities.

5.2 Geochemistry

The siliceous rocks mainly consist of SiO_2, with the SiO_2 contents vary from 96.87% to 97.9%, with an average of 97.24%, showing highly pure composition. The secondary constitute is Al_2O_3, and the content of the other elements are very low (Table 1). The Al/(Al+Fe+Mn) atomic ratio is an important indicator for evaluating the content of hydrothermal sedimentary components in various sediments, and the ratios decrease with increasing content of hydrothermal components. In addition, low TiO_2 content is the typical character of the hydrothermal siliceous rocks. In Shewushan deposit, the Al/(Al+Fe+Mn) ratios of our samples range from 0.244 to 0.317, and TiO_2 content is 0.01% (Table 1), showing the hydrothermal characteristics. In the Al-Fe-Mn triangle diagram, we plotted samples of Shewushan, West Qinling, Franciscan and Shimanto, showing their hydrothermal characteristics (Fig. 10).

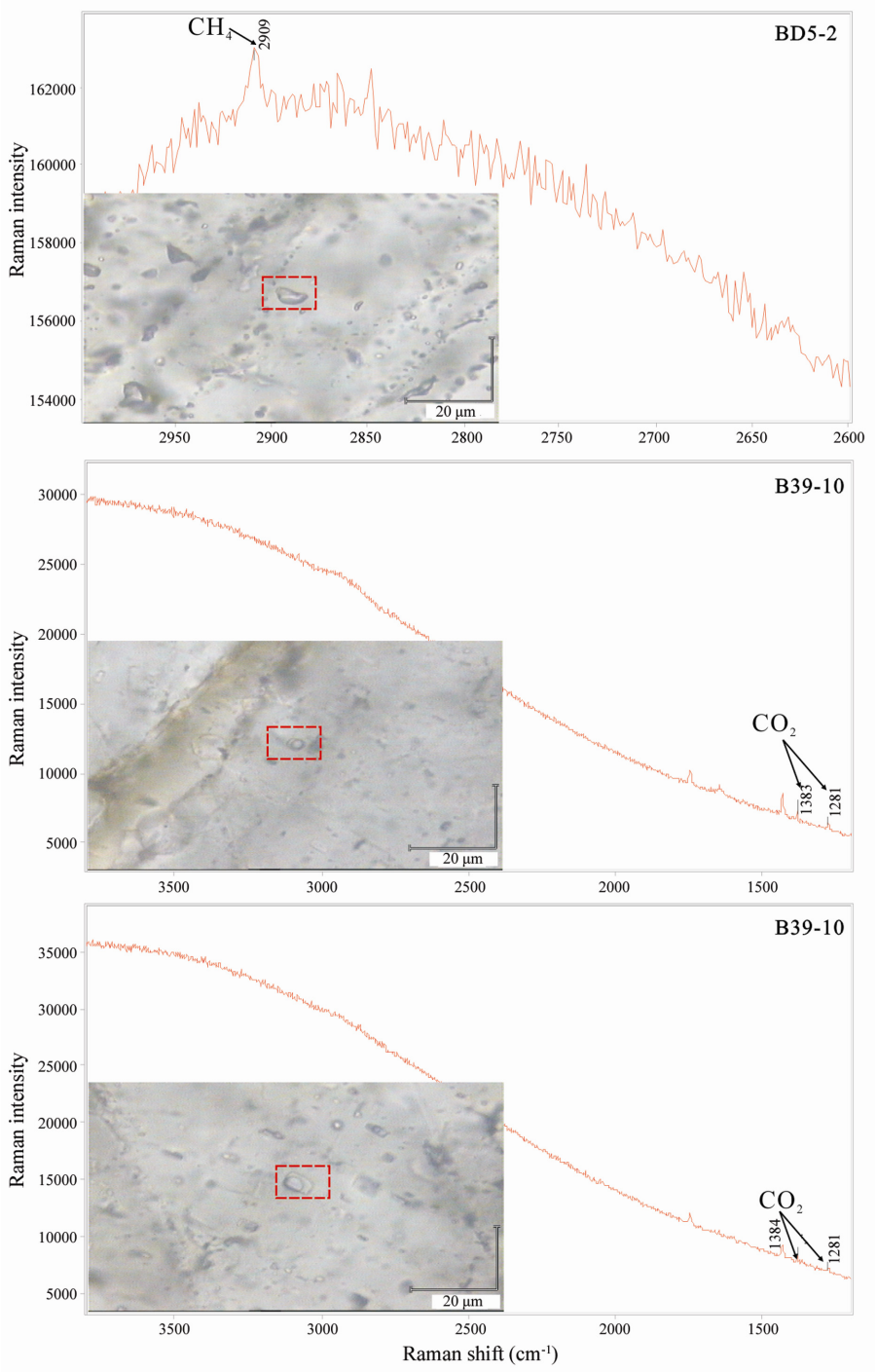

Fig. 9. Summary of representative Raman spectra with laser spot focused on individual phases in fluid inclusions (temperature: 25℃; moisture: 56%).

Table 1 Major element contents of the siliceous rocks from Shewushan gold deposit (%)

Sample	SiO_2	TiO_2	Al_2O_3	Fe_2O_3	FeO	MnO	MgO	CaO	Na_2O	K_2O	P_2O_5	Al/(Al+Fe+Mn)
HX07	97.90	0.01	0.30	0.54	0.38	0.01	0.06	0.01	0.10	0.04	0.013	0.244
BD05	96.87	0.01	0.44	0.69	0.25	0.01	0.06	0.01	0.11	0.05	0.020	0.317
West Qinling[1]	95.30	0.04	0.41	1.03	0.58	0.03	0.19	0.68	0.06	0.08	0.250	0.153
Franciscan[2]	92.30	0.09	1.31	0.27	2.36	0.53	0.28	0.11	0.16	0.35	0.030	0.293
Shimanto[3]	87.87	0.05	1.09	0.52	2.52	1.08	0.86	1.05	0.35	0.24	0.120	0.209

[1]Average composition of cherts from West Qinling, data from Liu Jiajun et al. (1999); [2, 3]data from Yamamoto (1987). Al/(Al+Fe+Mn)= $Al_2O_3/(Al_2O_3+Fe_2O_3+FeO+MnO)$.

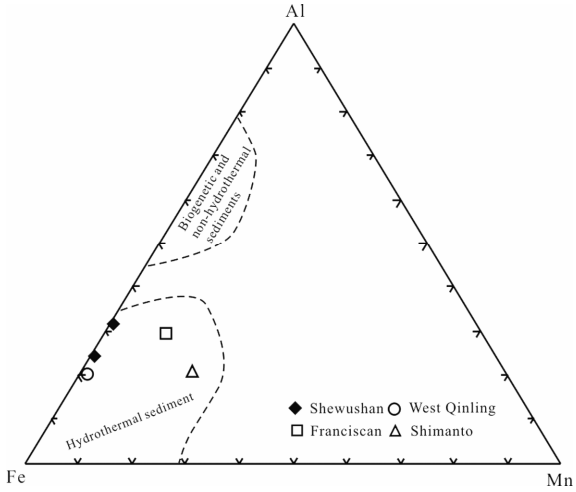

Fig. 10. Triangle diagram of Al-Fe-Mn in different rocks (based on Yamamoto, 1987 and Adachi et al., 1986).

Hydrothermal sediments are relatively enriched in Cu, Ni and depleted in Co (Crerar et al., 1982), and there are high contents of As, Ba and Sb in sediments (Bostroem et al., 1979; Marchig et al., 1982). In the U-Th diagram, the siliceous rocks fall into hydrothermal field (Fig. 11). In the triangle diagram of Fe-Mn-(Co+Ni+Cu)×10, the siliceous rocks fall into the hydrothermal field close to the Fe-end member (Fig. 12). Therefore, trace elements indicate that the siliceous rocks are hydrothermal sediments in the Shewushan gold deposit.

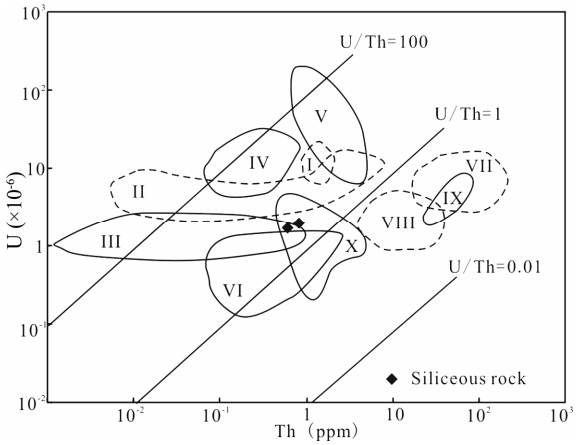

Fig. 11. Plot of U and Th of siliceous rocks in Shewushan deposit, after Bostroem et al.(1979). I. TAG hydrothermal area, at the Mid-Atlantic Ridge; II. Galapagos spreading center deposits; III. Amphitrite expedition, dredge site 2; IV. Red sea hot brine deposits; V. East Pacific Rise crest deposits; VI. Lanban hydrothermal sediments; VII. ordinary manganese nodules; VIII. ordinary pelagic sediments; IX. laterites; X. fossil hydrothermal deposits.

In addition, REE compositions are also the important indicators distinguishing hydrothermal sediments from non-hydrothermal sediments (Marchig et al., 1982). The total REE contents of the siliceous rocks vary from 3.575×10^{-6} to 11.347×10^{-6} (Table 2). LREE/HREE>1, the values of Eu anomaly (Eu/Eu^*) and Ce anomaly (Ce/Ce^*) vary from 0.365 to 0.630 and from 0.889 to 1.038, respectively. The REE patterns are right-inclined (Fig. 13), and a lack of negative Ce anomaly, which usually appears in marine hydrothermal cherts (Bostroem et al., 1979, 1983; Adachi et al., 1986; Yamamoto, 1987), showing these siliceous rocks formed in the continental depositional environment.

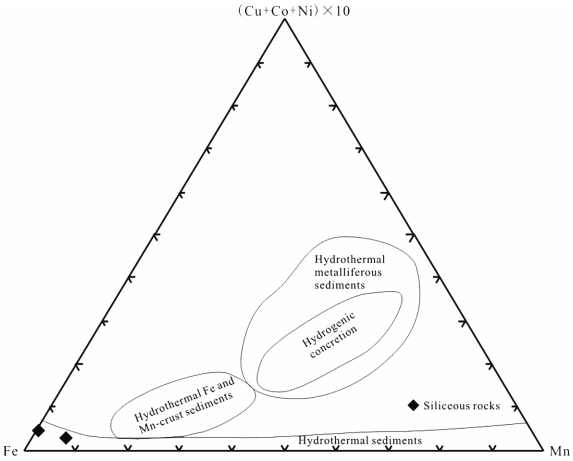

Fig. 12. Ternary diagram for Fe-Mn-(Cu+Co+Ni)×10 (modified after Crerar et al., 1982).

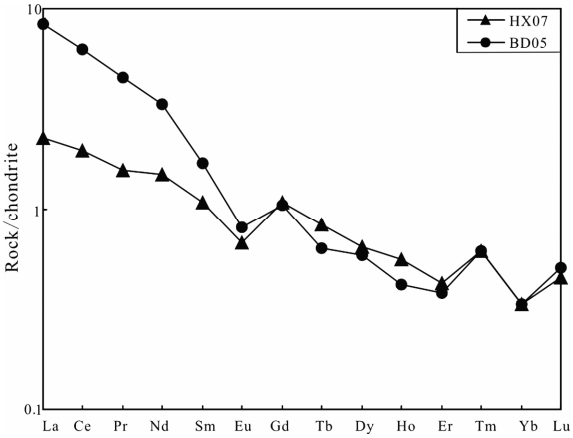

Fig. 13. REE pattern of siliceous rocks from Shewushan gold deposit.

6 Electron microprobe analysis

To make certain the occurrence of gold in Shewushan gold deposit, we choose EPMA to detect the elements content in pyrite and arsenopyrite. The chemical compositions were analyzed by electron microprobe analysis (JCXA-733, Japan) with five X-ray wavelength-dispersive spectrometers at the State Key Laboratory of Geological Processes and Mineral Resources, China University of Geosciences. Pyrite and

arsenopyrite were analyzed for Au, Ag, Co and Ni at 25 keV accelerating voltage and 10–40 nA beam current, keeping counting time of 10s.

The results show that gold is predominantly in arsenopyrite (850×10^{-6}–1550×10^{-6} Au), with lesser amounts in pyrite (470×10^{-6}–1340×10^{-6} Au) (Table 3). As we all know, the Co/Ni value in pyrite is the key index to confirm the pyrite genesis. The Co/Ni values range from 2.46 to 6.85, indicating its hydrothermal genesis. To some extent, Co content in pyrite could indicate the pyrite genesis: pyrite generated at high temperature pyrite has Co content higher than 1000×10^{-6}, and generated at middle temperature has Co content between 100×10^{-6} and 1000×10^{-6}, while at low temperature has Co content lower than 100×10^{-6}. The Co contents in pyrite range from 640×10^{-6} to 890×10^{-6} in Shewushan gold deposit, suggesting that pyrite was generated in middle temperature.

7 Discussion

Geochemistry of siliceous rock shows high As and Sb, with rarely sulfides, suggesting that gold may migrate through arsenic and antimony thio-sulfate complexes. Thio-sulfates of Au are soluble in water system (Mann, 1984). It is unstable in acid environment, where it is subject to disproportionation; while in alkaline solution it may be able to survive for thousands of years (Pryor, 1960). This means that thio-sulfate anions may be stable in pore networks of carbonates, which typically keep an elevated pH. The involvement of arsenic and antimony thio-sulfate in the migration of gold has been proposed (Boyle et al., 1975).

Table 2 REE contents in siliceous rocks from Shewushan Au deposit ($\times10^{-6}$)

Sample	La	Ce	Pr	Nd	Sm	Eu	Gd	Tb	Dy	Ho	Er	Tm	Yb	Lu
HX07	0.7	1.6	0.19	0.9	0.21	0.05	0.28	0.04	0.21	0.04	0.09	0.02	0.07	0.02
BD05	2.6	5.1	0.55	2.0	0.33	0.06	0.27	0.03	0.19	0.03	0.08	0.02	0.07	0.02
Chondrite	0.31	0.808	0.122	0.6	0.195	0.0735	0.259	0.0474	0.322	0.0718	0.21	0.0324	0.209	0.0332

Sample	∑REE	LREE	HREE	LREE/HREE	Eu/Eu*	Ce/Ce*	$(La/Yb)_N$	$(La/Sm)_N$	$(Gd/Yb)_N$
HX07	4.42	3.65	0.77	4.740	0.630	1.038	6.742	2.097	3.228
BD05	11.35	10.64	0.71	14.986	0.597	0.979	25.041	4.956	3.113

Note: Chondrite data from Boynton, 1984.

Table 3 EPMA results of Au, Ag, Co and Ni in pyrite and arsenopyrite from Shewushan gold deposit (wt.%)

Sample	Type	Point	Mineral	Size (μm)	Morphology	Au	Ag	Co	Ni
B11-1-1	Arsenopyrite vein	1	Arsenopyrite	30	Long strip	0.120	-	0.098	0.052
		2	Arsenopyrite	30	Long strip	0.106	0.019	0.101	0.082
		3	Arsenopyrite	30	Long strip	0.123	-	0.073	0.026
		4	Arsenopyrite	100	Lath	0.091	0.029	0.08	0.03
		5	Arsenopyrite	100	Lath	0.123	0.036	0.08	0.044
		6	Arsenopyrite	100	Lath	0.113	0.021	0.082	0.028
B39-3	Dolomitic limestone	1	Pyrite	500	Subeuhedral	0.112	0.008	0.076	0.018
		2	Pyrite	500	Subeuhedral	0.047	0.035	0.089	0.013
		3	Pyrite	500	Subeuhedral	0.125	0.021	0.088	0.014
		4	Pyrite	50	Subeuhedral	0.134	-	0.065	0.014
		5	Pyrite	50	Subeuhedral	0.078	-	0.068	0.01
		6	Pyrite	50	Subeuhedral	0.091	-	0.064	0.026
BD12	Dolomitic limestone	1	Arsenopyrite	20	Anhedral	0.085	0.012	0.092	0.025
		2	Arsenopyrite	20	Anhedral	0.124	0.01	0.063	0.012
		3	Arsenopyrite	20	Anhedral	0.121	0.004	0.081	0.024
		4	Arsenopyrite	20	Anhedral	0.104	-	0.082	0.028
B59-5-2	Breccia	1	Arsenopyrite	100	Euhedral	0.107	-	0.075	0.019
		2	Arsenopyrite	100	Euhedral	0.101	0.013	0.089	0.031
		3	Arsenopyrite	100	Euhedral	0.105	-	0.085	0.025
		4	Arsenopyrite	100	Euhedral	0.111	-	0.067	0.026
		5	Arsenopyrite	50	Anhedral	0.146	-	0.1	0.095
		6	Arsenopyrite	50	Anhedral	0.119	-	0.08	0.018

Note: - no data.

The source of the primary gold mineralization is conjectural. The predominant theory is that gold is scavenged from country sediments and redeposited above areas of high heat flow. As for Shewushan gold deposit, primary gold mineralization is attributed to hydrothermal activity that followed the main period of tectonic deformation of the Indosinian orogeny, which caused the regional detachment regime in southeast Hubei, the reversed fold and the fault system in the Shewushan area and formed the fluid migration channel. Moreover, the fault system may have supplied the heat to convert meteoric water with Au-Sb-As bearing solutions possibly being generated by scavenging metals from the carbonate sediments or their bedrock.

8 Conclusions

The homogenization temperature ranges from 110 to 290℃. The salinity varies from 2.2% to 9.34% *w* (NaCl, equivalent). The pressure falls in the range from 42 to 46 MPa, which indicates that the gold mineralization took place under the condition of low temperature, low pressure with low salinity hydrothermal fluid.

EPMA results show that primary mineralization is typified by gold-bearing arsenopyrite and pyrite and hosted by tectonic crushed clay-rich limestone, which is the typical gold-bearing mineral in carlin type gold deposit (Kuehn and Rose, 1992; Hu Ruizhong et al., 2002).

The geochemistry data of siliceous rock illustrate that it is hydrothermal sediments that is deposited near fault surface by bearing SiO_2 mineralized fluid migrates along the fault.

In summary, primary mineralization was structurally controlled and formed in closely association with the well-developed faults and fractures mainly on the crest of the reverse anticline, with approximately east-west axis, which is adhere to the geotectonic setting and metallogenic characteristics of carlin gold deposit in China (Liu Dongsheng, 1994). Also, the widely developed silification, argillaceous alteration and pervasive limonitization, mild pyritization and realgarization are the typical alteration of carlin gold deposit (Kuehn and Rose, 1992; Liu Dongsheng, 1994; Hu Ruizhong et al., 2002).

Therefore, in this study, deposit geology, mineralized fluid, and gold bearing minerals support the genesis of the primary orebody in Shewushan gold deposit is carlin type.

Acknowledgements This research project was financially supported jointly by the National Natural Science Foundation of China (No. 40902026, No. 41272097), the State Key Laboratory of Geological Processes and Mineral Resources (No. GPMR 201006), and the Special Fund for Basic Scientific Research of Central Colleges, China University of Geosciences (Wuhan) (No. CUG120702). We also appreciate the Shewushan Gold Mine Co. Ltd and No. 4 Geological Party, Hubei Bureau of Geology and Mineral Resources for the field support.

References

Adachi M., Yamamoto K., and Sugisaki R. (1986) Hydrothermal chert and associated siliceous rocks from the northern Pacific: Their geological significance as indication of ocean ridge activity [J]. *Sedimentary Geology*. **47**, 125–148.

Bodnar R. and Sterner S. (1987) Synthetic fluid inclusions. In *Hydrothermal Experimental Techniques* (eds. Ulmer G.C. and Barnes H.L.) [C]. pp.423–457. John Wiley & Sons, New York.

Bostroem K., Rydell H., and Joensuu O. (1979) Langban: An exhalative sedimentary deposit [J]. *Economic Geology and the Bulletin of the Society of Economic Geologists*. **74**, 1002–1011.

Bostroem K. (1983) Genesis of ferromanganese deposits-diagnostic criteria for recent and old deposits. In *Hydrothermal Processes at Seafloor Spreading Centers* (ed. Rona P.A.) [C]. pp.473–483. Plenum Press, New York.

Boyle R.W., Alexander W.M., and Aslin G.E. (1975) *Some Observations on the Solubility of Gold* [M]. pp.24–75. Geological Survey of Canada, Ottawa.

Boynton W.V. (1984) Cosmochemistry of the rare earth elements: Meteorite studies. In *Rare-Earth Element Geochemistry* (ed. Henderson P.) [C]. pp. 63–107. Elsevier, Amsterdam.

Cao Xinzhi (1998) Overview of research on laterite gold deposit in China [J]. *Geological Science and Technology Information*. **17**, 50–54 (in Chinese with English abstract).

Chen Dajing and Yang Mingshou (1999) Characteristics and models of lateritic gold deposit in South China [J]. *Geochemical Exploration for Non-ferrous Metals*. **8**, 651–652 (in Chinese).

Chen Dajing, Yang Mingshou, and Zhang Yonglin (2001) Geological characteristics and metallogenic model of the Zhenxu-type laterite gold deposits in Guangxi [J]. *Mineral Deposits*. **20**, 251–258 (in Chinese with English abstract).

Crerar D.A., Namson J., Chyi M.S., Williams L., and Feigenson M.D. (1982) Manganiferous cherts of the Franciscan assemblage: I, General geology, ancient and modern analogues, and implications for hydrothermal convection at oceanic spreading centers [J]. *Economic Geology and the Bulletin of the Society of Economic Geologists*. **77**, 519–540.

Davy R. (1979) Geochemical exploration, Saddleback greenstone belt, Western Australia [J]. *Western Australia Geological Survey*. **8**, 87.

Davy R. and El-Ansary M. (1986) Geochemical patterns in the laterite profile at the Boddington gold deposit, Western Australia [J]. *Journal of Geochemical Exploration*. **26**, 119–144.

Ding Qixiu (1992) Some new ideas on stratigraphy of Shewushan area [J]. *Hubei Geology*. **5**, 4–6 (in Chinese with English abstract).

Freyssinet P., Zeegers H., and Tardy Y. (1989) Morphology and geochem-

istry of gold grains in lateritic profiles of southern Mali [J]. *Journal of Geochemical Exploration*. **32**, 17–31.

Glasson M.J., Lehne R.W., and Wellmer F.W. (1988) Gold exploration in the callion area, eastern goldfields, western Australia [J]. *Journal of Geochemical Exploration*. **31**, 1-19.

Hong Hanlie (1996) Microscopic characteristics of the clay minerals in the oxidized zone of Shewushan gold mine in Jiayu, Hubei [J]. *Hubei Geology*. **10**, 71–74 (in Chinese with English abstract).

Hong Hanlie (2001) Weathered mantle hosted gold deposit at Shewushan, Hubei, Central China [J]. *Journal of China University of Geosciences*. **12**, 60–67.

Hong Hanlie, Bian Qiujuan, and Wang Qinyan (2000) Supergene ore and hypogene sub-economic gold mineralization at Shewushan, Hubei, central China [J]. *Applied Earth Science*. **109**, 196–198.

Hong Hanlie and Tie Liyun (2005) Characteristics of the minerals associated with gold in the Shewushan supergene gold deposit, China [J]. *Clays and Clay Minerals*. **53**, 162–170.

Hong Hanlie, Wang Qinyan, Chang Jianping, Liu Shirong, and Hu Ruizhong (1999) Occurrence and distribution of invisible gold in the Shewushan supergene gold deposit, southeastern Hubei, China [J]. *Canadian Mineralogist*. **37**, 1525–1532.

Hu Ruizhong, Su Wenchao, Bi Xianwu, Tu Guangchi, and Albert H. (2002) Geology and geochemistry of Carlin-type gold deposits in China [J]. *Mineralium Deposita*. **37**, 378-392.

Kuehn C.A. and Rose A.W. (1992) Geology and geochemistry of wall-rock alteration at the Carlin gold deposit, Nevada [J]. *Economic Geology* **87,** 1697–1721.

Larizzatti J.H., Oliveira S.M.B., and Butt C.R.M. (2008) Morphology and composition of gold in a lateritic profile, Fazenda Pison "Garimpo", Amazon, Brazil [J]. *Journal of South American Earth Sciences*. **25**, 359–376.

Li Jiaxiang and Liu Shimin (1995) The geological characteristics of Carlin type gold deposit in Shewushan, Hubei Province [J]. *Hubei Geology*. **9**, 91–99 (in Chinese with English abstract).

Li Jiangyuan, Pen, Jingling, Luo Bin, and Luo Xiangsheng (1994) The geological characteristics of laterite gold ore of Shewushan type in Hubei [J]. *Hubei Geology*. **8**, 25–33 (in Chinese with English abstract).

Li Songsheng (1993) The geology and genesis of Shewushan laterite gold deposit, Hubei [J]. *Geology and Exploration*. **29**, 12–15 (in Chinese).

Li Songsheng (1998) A further discussion on the genesis of the Shewushan lateritic gold deposit [J]. *Mineral Deposits*. **17**, 114–124 (in Chinese with English abstract).

Li Wenda and Chen Zhongfu (1994) *Geochemistry of Laterization in South China and Possibility for Lateritic Type Gold Deposit Forming* [M]. pp.1–88. Geological Publish House, Beijing (in Chinese with English abstract).

Lima da Costa M. (1993) Gold distribution in lateritic profiles in South America, Africa, and Australia: Applications to geochemical exploration in tropical regions [J]. *Journal of Geochemical Exploration*. **47**, 143–163.

Liu Jiajun, Zheng Minghua, Liu Jianming, Zhou Yufeng, Gu Xuexiang, and Zhang Bin (1999) The geological and geochemical characteristics of Cambrian chert and their sedimentary enviromental implication in western Qinling [J]. *Acta Petrologica Sinica*. **15**, 145–154.

Liu Shimin and Li Jiaxiang (1995) Geology and genesis of Shewushan carlin type of gold deposit in Hubei Province [J]. *Journal of Precious Metallic Geology*. **4**, 184–192 (in Chinese with English abstract).

Liu Tengfei (1996) Geological feature and exploration of lateritic gold deposit in Shewushan, Hubei [J]. *Gold Geology*. **2**, 25–30 (in Chinese with English abstract).

Mann A.W. (1984) Mobility of gold and silver in lateritic weathering profiles; some observations from Western Australia [J]. *Economic Geology.* **79**, 38–49.

Marchig V., Gundlach H., Möller P., and Schley F. (1982) Some geochemical indicators for discrimination between diagenetic and hydrothermal metalliferous sediments [J]. *Mar Geololy.* **50**, 241–256.

Marcondes L.d.C. (1993) Gold distribution in lateritic profiles in South America, Africa, and Australia: Applications to geochemical exploration in tropical regions [J]. *Journal of Geochemical Exploration*. **47**, 143–163.

Porto C.G. and Hale M. (1995) Gold redistribution in the stone line lateritic profile of the Posse deposit, Central Brazil [J]. *Economic Geology and the Bulletin of the Society of Economic Geologists.* **90**, 308–321.

Pryor W.A. (1960) The kinetics of the disproportionation of sodium thiosulfate to sodium sulfide and sulfate [J]. *Journal of the American Chemical Society*. **82**, 4794–4797.

Santosh M. and Omana P.K. (1991) Very high purity gold form lateritic weathering profiles of Nilambur, southern India [J]. *Geology*. **19**, 746–749.

Tu Guangchi (1999) Some discussions on precious metal prospecting. In *Theories Methods Mineral Resources Prospecting Evaluation.* (ed. Chen Y.C.) [C]. pp.186–191. Seismic Publishing House, Beijing (in Chinese with English abstract).

Varajão C.A.C., Colin F., Vieillard P., Melfi A.J., and Nahon D. (2000) Early weathering of palladium gold under lateritic conditions, Maquiné Mine, Minas Gerais, Brazil [J]. *Applied Geochemistry.* **15**, 245–263.

Wang Tong and Yang Mingai (1992) A preliminary study on the occurrence of gold in primary ore from Shewushan gold deposit [J]. *Hubei Geology*. **6**, 40–46 (in Chinese with English abstract).

Wang Yan and Tan Kaixuan (2002) Ore-forming mechanism and model of lateritic gold deposits [J]. *Geology and Prospecting*. **38**, 12–16 (in Chinese with English abstract).

Yamamoto K. (1987) Geochemical characteristics and depositional environments of cherts and associated rocks in the Franciscan and Shimanto Terranes [J]. *Sedimentary Geology.* **52**, 65–108.

Yang Yuangen, Liu Shirong, and Jin Zhisheng (2009) Laterization and its control to gold occurrence in Laowanchang gold deposit, Guizhou Province, Southwest of China [J]. *Journal of Geochemical Exploration*. **100**, 67–74.

Yu Renyu (1994) Geological characteristics and genesis of the weathering type gold deposit in the Shewushan gold ore district, Hubei Province [J]. *Mineral Deposits*. **13**, 28–37 (in Chinese with English abstract).

Yu Renyu (1996) Geological conditions and mechanism of metallization of a large-scale laterite-type gold deposit [J]. *Geology and Prospecting*. **32**, 1–6 (in Chinese with English abstract).

Zang Weisheng and Fyfe W.S. (1993) A three-stage genetic model for the Igarape Bahia lateritic gold deposit, Carajas, Brazil [J]. *Economic Geology and the Bulletin of the Society of Economic Geologists.* **88**, 1768–1779.